

Nonlinear FEA of higher order beam resting on a tensionless foundation with friction

Guanghai He¹, Xiaowei Li² and Rong Lou^{*1}

¹ School of Maritime and Civil Engineering, Zhejiang Ocean University, Zhoushan, China

² Songjiang Campus of Shanghai Open University, Shanghai, China

(Received November 21, 2015, Revised March 28, 2016, Accepted March 28, 2016)

Abstract. A novel higher order shear-deformable beam model, which provides linear variation of transversal normal strain and quadratic variation of shearing strain, is proposed to describe the beam resting on foundation. Then, the traditional two-parameter Pasternak foundation model is modified to capture the effects of the axial deformation of beam. The Masing's friction law is incorporated to deal with nonlinear interaction between the foundation and the beam bottom, and the nonlinear properties of the beam material are also considered. To solve the mathematical problem, a displacement-based finite element is formulated, and the reliability of the proposed model is verified. Finally, numerical examples are presented to study the effects of the interfacial friction between the beam and foundation, and the mechanical behavior due to the tensionless characteristics of the foundation is also examined. Numerical results indicate that the effects of tensionless characteristics of foundation and the interfacial friction have significant influences on the mechanical behavior of the beam-foundation system.

Keywords: nonlinear quasi-static analysis; Pasternak foundation; Masing's friction law; higher order beam model; finite element method

1. Introduction

The beam-foundation system is commonly used in the civil engineering. Many types of structures, including the railway tracks resting on the half space soil, the piles embedded in the soil and the strip foundation beam supporting the building, can be catalogued to the beam-foundation system. There are several simplified interaction models for engineering design and mechanical analysis of beam-foundation system. Winkler's model (Winkler 1867), which simplifies the soil as a single layer of vertically placed independent springs, may be the simplest one. The springs are modeled by a constant elastic stiffness coefficient or nonlinear p - y curve (Georgiadis and Georgiadis 2012), where the interaction among the springs is neglected. To refine the fidelity to the physical essence, several more refined models (Feng and Cook 1983), such as the Pasternak's model (Chen *et al.* 2004), Generalized foundation model (Nogami and O'Neill 1985) and the Vlasov foundation model (Jones and Xenophontos 1977), had been proposed to capture more elaborate mechanical behavior of the foundation. The common feature (Feng and Cook 1983) in these refined models is that they generally introduce another parameter to evaluate the effects of

*Corresponding author, Ph.D., E-mail: ghost261412@163.com

the shear interaction between the foundation and the beam bottom. Usually, the additional parameter is a constant coefficient for the linear foundation and t - z curve (Dash *et al.* 2009) for the nonlinear one. Due to the simplicity, these types of modeling still prevail (Dutta and Roy 2002, Ayoub 2003, Dash *et al.* 2009, Mullapudi and Ayoub 2010, Comodromos and Papadopoulou 2013) in the engineering practice. However, to the best knowledge of the authors, the interaction between structure and foundation is a contact problem (Berger 2002) and the friction effects (Berger 2002) between them is inevitable. To deal with this problem, the Coulomb's friction law (Popp *et al.* 2003) was initially proposed to formulate the interaction, and many other friction models were basically developed from his model, e.g., Masing model (Masing 1923) which incorporated an additional initial elastic deformable range to the Coulomb's model, and the generalized Maxwell slip model (Al-Bender *et al.* 2005) which took the viscosity into account. Comodromos and Bareka (2005) used the Coulomb's friction law for the interface modeling to study the negative skin friction effects using a 3D numerical model. Furthermore, Zhou *et al.* (2011) employed the Coulomb's friction law to describe the horizontal interfacial interaction between the beam and foundation, and studied the bending behavior of an elastic beam resting on the elastic Winkler foundation.

Classical beam models, like the Euler-Bernoulli beam model (Han *et al.* 1999) and the Timoshenko beam model (Han *et al.* 1999), have received a wide range of applications and are usually applied to the beam-foundation system (Ayoub 2003, Mullapudi and Ayoub 2010, Sapountzakis and Kampitsis 2013). However, it is unable to perform the detailed stress analysis of the beam, due to the over-simplified kinematics of the classical beam theory. In light of the higher order beam theory (HBT), which is free of this drawback and follows more refined kinematics yet holds lower spatial dimension than the 2D model, the authors believe that it is worthy of application of the HBT to the beam-foundation system to capture a reasonable shearing stress on the beam-foundation interface, and consequently take well into account the interfacial friction.

In this study, a modification to the Pasternak model is further made in two aspects. First, a novel higher order shear deformable beam model, which provides linear variation of transversal normal strain and quadratic variation of shearing strain, is proposed. Being different from the classical beam model, the new model is composed of seven basic unknown functions, instead of three the Timoshenko model holds. Due to the refined kinematics, the more detailed stress can be obtained and a more reliable interfacial friction can therefore be captured. Second, the aforementioned Masing's friction model (Masing 1923) is applied to the system. As the friction occurs only when the friction pair is in pressure, the present study follows the assumption that the foundation is tensionless, which is also a key issue attracting a considerable amount of investigators (Mullapudi and Ayoub 2010, Sapountzakis and Kampitsis 2011a, b, 2013, Nobili 2013, Zhang and Murphy 2013) to be devoted to, fairly recently. Furthermore, the nonlinear material properties of the beam and the p - y curves are considered. To carry out the analyses of the proposed new model, a new type of beam-foundation finite element is formulated, and the corresponding finite element program is verified by comparing the results with those based on the plane stress model and Refs. (Shirima and Giger 1992, Mullapudi and Ayoub 2010) in the linear range. The performance of the finite element program on nonlinear problem is also verified by the comparison with the results of Sapountzakis and Kampitsis (2013). Finally, extensive numerical examples of quasi-static analyses are performed, using the displacement incremental technique (Batoz and Dhett 1979) and modified Newton-Raphson correction method (Zienkiewicz and Taylor 2000) to illustrate the influences of tensionless characteristics and friction on the mechanical behavior of beam-foundation system.

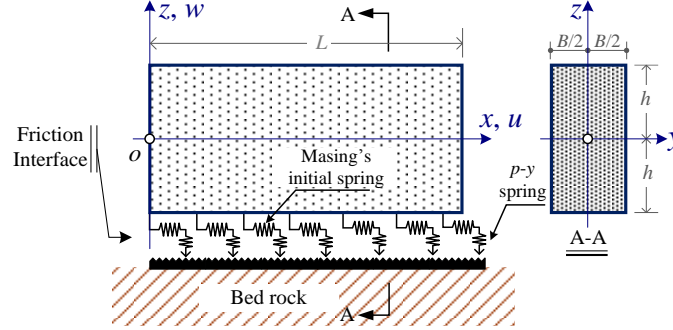


Fig. 1 A rectangular beam resting on a foundation

2. Statement of the problem

2.1 Higher order beam model

2.1.1 Kinematics

As is shown in Fig. 1, a beam with rectangular cross-section $B \times 2h$ is resting on a foundation, and an ox coordinate axis is set from the centroid of the cross-section at the left end of the beam. To obtain more refined displacements and stress results, we assume that the axial displacement $u(x, z)$ and transversal displacement $w(x, z)$ of the beam can be approximated, respectively, as

$$u(x, z) = u_0(x) + u_1(x)z + u_2(x)z^2 + u_3(x)z^3 \quad (1)$$

$$w(x, z) = w_0(x) + w_1(x)z + w_2(x)z^2 \quad (2)$$

where u_i and w_j ($i = 0, 1, 2, 3; j = 0, 1, 2$), are the basic unknown functions to be solved. Compared with Timoshenko beam model, $u_0(x)$ and $u_1(x)$ herein can be interpreted as the axial displacement and the cross-sectional rotation at the centroid of the cross-section, respectively; $w_0(x)$ serves as the deflection of the cross-sectional centroid, while the rest terms in Eqs. (1)-(2) are neglected by classical beam models like Timoshenko and Euler-Bernoulli.

2.1.2 Geometric equations

The beam-foundation system is supposed to have small displacements when subjected to the external loads, thus, the geometric equations based on the linear elasticity still hold. From Eqs. (1)-(2), the strain fields of the higher order beam can be derived as

$$\varepsilon_x = \frac{\partial u}{\partial x} \equiv u_0'(x) + u_1'(x)z + u_2'(x)z^2 + u_3'(x)z^3 \quad (3)$$

$$\gamma_{xz} = \frac{\partial u}{\partial z} + \frac{\partial w}{\partial x} \equiv u_1(x) + 2zu_2(x) + 3z^2u_3(x) + w_0'(x) + w_1'(x)z + w_2'(x)z^2 \quad (4)$$

herein the prime ' denotes the derivative with respect to x , i.e., $(\square)' = d(\square)/dx$; ε_x and γ_{xz} indicate normal strain and shearing strain of the higher order beam, respectively.

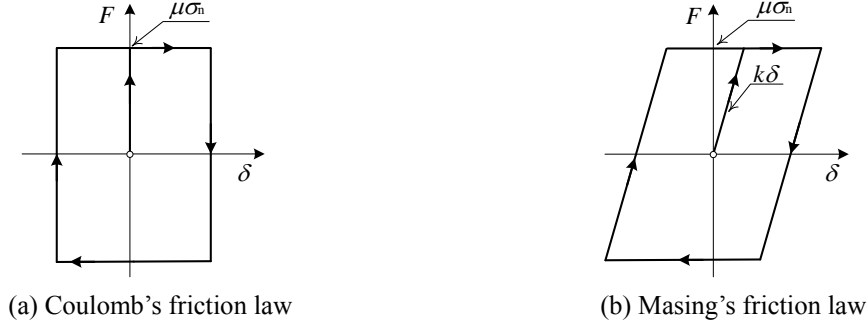


Fig. 2 Friction hysteresis loop

2.2 Material and friction models

2.2.1 Friction models

Coulomb's friction law (see Fig. 2(a)) is one of the earliest friction models, which assumes that the sliding friction force is proportional to the pressure σ_n between the friction pair, and the direction of the friction force is opposite to the relative slide δ . Specifically, the symbol μ , as is shown in Figs. 2(a) and (b), denotes the friction coefficient. Despite the simplicity, this model has received a wide range of applications to the civil engineering.

Aiming to capture the sticking state of the friction pair, we assume that there is a linear elastic stage as given by Masing's friction law, and it is illustrated in Fig. 2(b) as $F = k\delta$. In this stage, as the deformation is very small, the beam bottom and the soil in contact are both assumed to be elastic and will deform, although the deformation range is very small. This stage is in accordance with Pasternak's foundation model, because the elastic stiffness coefficient k shown in Fig. 2(b) is just corresponding to the Pasternak's second foundation parameter. The Masing's friction law is thus chosen to formulate the interfacial friction in this study.

2.2.2 Beam materials

Both the linear-elastic plane stress and nonlinear-elastic models are considered in this study. The constitutive relation for the former one can be written as

$$[\sigma_x \quad \sigma_z \quad \tau_{xz}]^T = \mathbf{D}[\varepsilon_x \quad \varepsilon_z \quad \gamma_{xz}]^T \quad (5)$$

where

$$\mathbf{D} = \begin{bmatrix} \frac{E}{1-\nu^2} & \frac{E\nu}{1-\nu^2} & 0 \\ \frac{E\nu}{1-\nu^2} & \frac{E}{1-\nu^2} & 0 \\ 0 & 0 & \frac{E}{2(1+\nu)} \end{bmatrix} \quad (6)$$

herein E and ν indicate the Young's modulus and Poisson's ratio, respectively.

For nonlinear beam materials, the constitutive relation can be written as

$$\sigma_x = f_1(\varepsilon_x), \quad \sigma_z = f_1(\varepsilon_z), \quad \tau_{xz} = f_2(\gamma_{xz}) \quad (7)$$

in which, the normal stresses σ_x and σ_z are governed by the same nonlinear function f_1 , and the nonlinear function f_2 describes the behavior of shear deformation.

3. Finite element formulations

3.1 Principle of virtual work

Generally, the principle of virtual work of the beam-foundation system may be formulated as

$$\begin{aligned} & \int_{\Omega} [(\delta\varepsilon_x)\sigma_x + (\delta\varepsilon_z)\sigma_z + (\delta\gamma_{xz})\tau_{xz}] d\Omega + \int_{\Gamma_b} \{[\delta u(x, -h)]F_1 + [\delta w(x, -h)]F_2\} d\Gamma_b \\ & = \int_{\Gamma_t} \{-[\delta w(x, h)]q(x) + [\delta u(x, h)]T(x)\} d\Gamma_t + [\delta w(x_0, h)]P_0 + [\delta u(x_0, h)]T_0 \end{aligned} \quad (8)$$

where Γ_b and Γ_t indicate the bottom and top surfaces of the beam, respectively; Ω is the domain the foundation beam occupies; $q(x)$ and $T(x)$ (see Fig. 3) are the external distributed pressure and traction, and P_0 and T_0 are the point load acting on the top surface with distance x_0 from the left end of the beam; F_1 and F_2 (see Fig. 3) are the friction force and pressure acting on the bottom surface of the beam.

3.2 Shape functions

A displacement-based finite element (see Fig. 4) with three nodes marked with 1, 2, and 3 is constructed for higher order foundation beam, where each node possesses seven DOFs: $u_0^{(n)}$, $u_1^{(n)}$, $u_2^{(n)}$, $u_3^{(n)}$, $w_0^{(n)}$, $w_1^{(n)}$ and $w_2^{(n)}$, $n = 1, 2, 3$. The nodal DOF vector for this element is defined as

$$\delta_e = [\Psi^{(1)} \quad \Psi^{(2)} \quad \Psi^{(3)}]^T \quad (9)$$

in which $\Psi^{(n)} = [u_0^{(n)} \quad u_1^{(n)} \quad u_2^{(n)} \quad u_3^{(n)} \quad w_0^{(n)} \quad w_1^{(n)} \quad w_2^{(n)}], n = 1, 2, 3$.

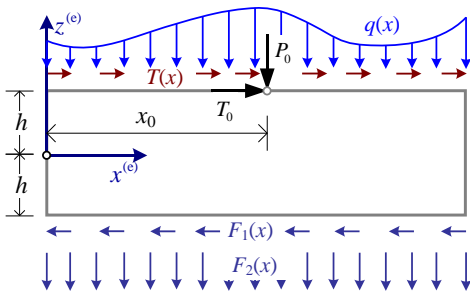


Fig. 3 Beam subjected to the external load

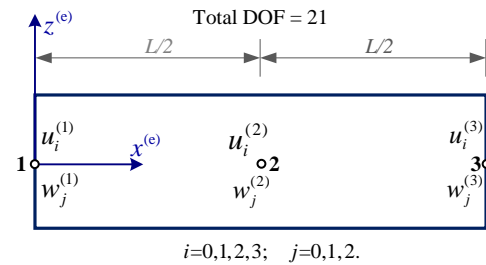


Fig. 4 Nodal DOF of the higher order beam element

The shape functions for the basic unknowns can be conventionally derived by using Lagrange interpolation bases. And the finite element approximation of the unknown functions may be obtained as

$$u_j^h = \sum_{i=1}^3 N_i u_j^{(i)}, \quad w_k^h = \sum_{i=1}^3 N_i w_k^{(i)}, \quad j=0, 1, 2, 3. \quad k=0, 1, 2. \quad (10)$$

where shape functions $N_1 = (2x - L)(x - L) / L^2$ and $N_3 = x(2x - L) / L^2$; hereafter the apex ‘h’ denotes the finite element approximation.

Combining Eqs. (9)-(10) leads to

$$u_i^h = \mathbf{N}_{ui} \boldsymbol{\delta}_e, \quad w_j^h = \mathbf{N}_{wj} \boldsymbol{\delta}_e, \quad i=0, 1, 2, 3. \quad j=0, 1, 2. \quad (11)$$

where $[\mathbf{N}_{u0}^T \quad \mathbf{N}_{u1}^T \quad \mathbf{N}_{u2}^T \quad \mathbf{N}_{u3}^T \quad \mathbf{N}_{w0}^T \quad \mathbf{N}_{w1}^T \quad \mathbf{N}_{w2}^T]^2 = [N_1 \mathbf{I}_7 \quad N_2 \mathbf{I}_7 \quad N_3 \mathbf{I}_7]$, and \mathbf{I}_7 is a seventh order identity matrix.

Subsequently, finite element approximations for the displacement fields u and w can be derived using Eq. (11) as

$$u^h = \mathbf{N}_u \boldsymbol{\delta}_e, \quad w^h = \mathbf{N}_w \boldsymbol{\delta}_e \quad (12)$$

in which, $\mathbf{N}_u = \mathbf{N}_{u0} + z\mathbf{N}_{u1} + z^2\mathbf{N}_{u2} + z^3\mathbf{N}_{u3}$ and $\mathbf{N}_w = \mathbf{N}_{w0} + z\mathbf{N}_{w1} + z^2\mathbf{N}_{w2}$.

Consequently, finite element approximation for strain fields can be obtained as

$$\boldsymbol{\varepsilon}_x^h = \mathbf{N}_{\varepsilon x} \boldsymbol{\delta}_e, \quad \boldsymbol{\varepsilon}_z^h = \mathbf{N}_{\varepsilon z} \boldsymbol{\delta}_e, \quad \boldsymbol{\gamma}_{xz}^h = \mathbf{N}_{\gamma_{xz}} \boldsymbol{\delta}_e \quad (13)$$

with $\mathbf{N}_{\varepsilon x} = \frac{\partial \mathbf{N}_u}{\partial x}$, $\mathbf{N}_{\varepsilon z} = \frac{\partial \mathbf{N}_w}{\partial z}$, $\mathbf{N}_{\gamma_{xz}} = \frac{\partial \mathbf{N}_u}{\partial z} + \frac{\partial \mathbf{N}_w}{\partial x}$

3.3 Discrete finite element equations

Substituting Eqs. (12)-(13) into Eq. (8) yields

$$\begin{aligned} & \boldsymbol{\delta}_e^T \int_{\Omega} [\mathbf{N}_{\varepsilon x}^T \boldsymbol{\sigma}_x + \mathbf{N}_{\varepsilon z}^T \boldsymbol{\sigma}_z + \mathbf{N}_{\gamma_{xz}}^T \boldsymbol{\tau}_{xz}] d\Omega + \boldsymbol{\delta}_e^T \int_{\Gamma_b} \left\{ [\mathbf{N}_u^T(x, -h)] F_1 + [\mathbf{N}_w^T(x, -h)] F_2 \right\} d\Gamma_b \\ & = \boldsymbol{\delta}_e^T \int_{\Gamma_t} \left\{ -[\mathbf{N}_w^T(x, h)] q(x) + [\mathbf{N}_u^T(x, h)] T(x) \right\} d\Gamma_t + \boldsymbol{\delta}_e^T [\mathbf{N}_w^T(x_0, h)] P_0 + \boldsymbol{\delta}_e^T [\mathbf{N}_u^T(x_0, h)] T_0 \end{aligned} \quad (14)$$

Due to the arbitrariness of $\boldsymbol{\delta}_e^T$, Eq. (14) can be turned into an equivalent residual equation

$$\mathbf{res} \equiv \mathbf{F}_{\text{int}} - \mathbf{R}_{\text{ext}} = \mathbf{0} \quad (15)$$

where

$$\mathbf{F}_{\text{int}} = \int_{\Omega} [\mathbf{N}_{\varepsilon x}^T \boldsymbol{\sigma}_x + \mathbf{N}_{\varepsilon z}^T \boldsymbol{\sigma}_z + \mathbf{N}_{\gamma_{xz}}^T \boldsymbol{\tau}_{xz}] d\Omega + \int_{\Gamma_b} \left\{ [\mathbf{N}_u^T(x, -h)] F_1 + [\mathbf{N}_w^T(x, -h)] F_2 \right\} d\Gamma_b \quad (16)$$

$$\mathbf{R}_{\text{ext}} = \int_{\Gamma_t} \left\{ -[\mathbf{N}_w^T(x, h)] q(x) + [\mathbf{N}_u^T(x, h)] T(x) \right\} d\Gamma_t + [\mathbf{N}_w^T(x_0, h)] P_0 + [\mathbf{N}_u^T(x_0, h)] T_0 \quad (17)$$

When the beam materials are nonlinear and/or the nonlinear interaction of the system is considered, the residual Eq. (15) can't be solved directly, and an iteration technique is required. Herein, the Newton-Raphson (N-R) type iteration method is applied. Conventionally, the Jacobi matrix of residual vector Eq. (15), i.e., the tangential stiffness matrix, can be derived as

$$\mathbf{K}_t = \frac{\partial \mathbf{res}}{\partial \bar{\boldsymbol{\delta}}_e} = \int_{\Omega} \left[\mathbf{N}_{\varepsilon x}^T \frac{df_1}{d\varepsilon_x} \mathbf{N}_{\varepsilon x} + \mathbf{N}_{\varepsilon z}^T \frac{df_1}{d\varepsilon_z} \mathbf{N}_{\varepsilon z} + \mathbf{N}_{\gamma xz}^T \frac{df_2}{d\gamma_{xz}} \mathbf{N}_{\gamma xz} \right] d\Omega + \int_{\Gamma_b} \left\{ \left[\mathbf{N}_u^T(x, -h) \right] \frac{dF_1}{d\delta} \mathbf{N}_u(x, -h) + \left[\mathbf{N}_w^T(x, -h) \right] \frac{dF_2}{dw} \mathbf{N}_w(x, -h) \right\} d\Gamma_b \quad (18)$$

Then, the *N-R* correction procedure can be summarized as

$$\begin{cases} \bar{\mathbf{K}}_t^{(m)} \Delta \bar{\boldsymbol{\delta}}^{(m+1)} = \bar{\mathbf{R}}_{\text{ext}}^{(m)} - \bar{\mathbf{F}}_{\text{int}}^{(m)} \\ \bar{\boldsymbol{\delta}}^{(m+1)} = \bar{\boldsymbol{\delta}}^{(m)} + \Delta \bar{\boldsymbol{\delta}}^{(m+1)}, \quad m = 0, 1, 2, \dots \end{cases} \quad (19)$$

Hereafter the superscript ‘-’ denotes that the quantity is global, i.e., assembled from the element quantity. The indicator $\langle m \rangle$ indicates the m th converged solution. The initial value $\bar{\boldsymbol{\delta}}^{(0)}$ tends to be a zero vector or the last converged solution of the previously applied load case.

For a load controlled algorithm (Zienkiewicz and Taylor 2000), algorithm Eq. (19) is capable to implement and solve, if the external load is assigned to increase step by step. For the displacement controlled algorithm (Batoz and Dhatt 1979), there is an extra factor to multiply with the representative load vector, and this factor serves as an unknown. Accordingly, the value of the specified DOF of the system is incrementally prescribed. Therefore, the total sum of unknowns remains unchanged. In this study, both load and displacement controlled program are developed to carry out the coming numerical analysis.

The finite element equation will become a linear algebraic problem, when the beam materials are governed by Eq. (5) and the Pasternak's foundation model is applied, that is

$$F_1 = k_p \delta, \quad F_2 = k_w w \quad (20)$$

where k_p and k_w indicate the stiffness coefficients of the longitudinal and transverse spring, respectively; δ and w are the relative longitudinal and transverse displacement of the friction pair, respectively; F_1 and F_2 are the elastic resistance.

By using these linear models, the linear discrete finite element equation can be determined as

$$\mathbf{K}_e \bar{\boldsymbol{\delta}}_e = \mathbf{R}_e \quad (21)$$

where the element stiffness matrix \mathbf{K}_e and element load vector \mathbf{R}_e are evaluated from

$$\mathbf{K}_e = \int_{\Omega} \left[\mathbf{N}_{\varepsilon x}^T \left(\frac{E}{1-\nu^2} \mathbf{N}_{\varepsilon x} + \frac{\nu E}{1-\nu^2} \mathbf{N}_{\varepsilon z} \right) + \mathbf{N}_{\varepsilon z}^T \left(\frac{E}{1-\nu^2} \mathbf{N}_{\varepsilon z} + \frac{\nu E}{1-\nu^2} \mathbf{N}_{\varepsilon x} \right) + \mathbf{N}_{\gamma xz}^T \mathbf{GN}_{\gamma xz} \right] d\Omega + \int_{\Gamma_b} \left\{ \left[\mathbf{N}_u^T(x, -h) \right] k_p \mathbf{N}_u(x, -h) + \left[\mathbf{N}_w^T(x, -h) \right] k_w \mathbf{N}_w(x, -h) \right\} d\Gamma_b \quad (22)$$

$$\mathbf{R}_e = \int_{\Gamma_t} \left\{ -[\mathbf{N}_w^T(x, h)]q(x) + [\mathbf{N}_u^T(x, h)]T(x) \right\} d\Gamma_t + [\mathbf{N}_w^T(x_0, h)]P_0 + [\mathbf{N}_u^T(x_0, h)]T_0 \quad (23)$$

By the process of assembly (Zienkiewicz and Taylor 2000) and introduction of essential boundary conditions, the global discrete finite element equations for static analysis can be obtained as $\mathbf{K}\bar{\delta} = \mathbf{R}$, where \mathbf{K} and \mathbf{R} are the global elastic stiffness matrix and global load vector, respectively; $\bar{\delta}$ is the global displacement vector to be solved.

4. Numerical verification and analysis

4.1 Convergence test and shear effects

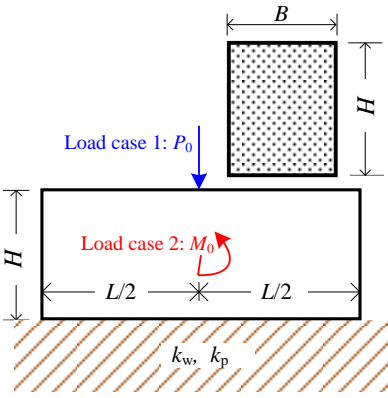
4.1.1 Convergence test

In this section, the convergence performance of the present finite element is examined through a linear analysis of a beam with free-free boundary conditions resting on a Pasternak foundation (see Table 1). The detailed geometric and physical parameters for this test are also tabulated in Table 1. The analytical solutions (see Appendix A for details) based on Timoshenko beam theory (TBT) and Euler-Bernoulli beam theory (EBT) are also presented as a comparison counterpart. There are two optional load cases tabulated in Table 1, and only the load case 1 is used in the convergence test. To take well into account the need of mesh refinement in the vicinity where the point load is applied, a meshing density formula is proposed as

$$l_i = \frac{1}{\beta + \text{Gaussian}(x_i, \bar{\mu}, \bar{\sigma})} \frac{L}{S}, \quad S = \sum_{i=1}^{n_e} \frac{1}{\beta + \text{Gaussian}(x_i, \bar{\mu}, \bar{\sigma})} \quad (24)$$

where, $\text{Gaussian}(x_i, \bar{\mu}, \bar{\sigma})$ is the normal distribution probability density function, with $\bar{\mu}$ the mean of the distribution, and $\bar{\sigma}$ the standard deviation. Herein L , as is given in Table 1, is the length of the foundation beam; n_e is the element number; for the i th element $x_i = iL / (n_e - 1)$ from the left end of the beam to the right, the element length is l_i .

Table 1 Structural parameters for the linear example 1 (Shirima and Giger 1992)

	Beam	Length L [m]	5.0
		Young's modulus E [GPa]	10.5
		Poisson's ratio ν	0.25
		Width B [m]	0.4
		Height H [m]	1.0
Foundation	Winkler's Parameter k_w [MPa]	3.081	
	Pasternak Parameter k_p [MPa]	49.796	
Load case 1	Concentrated force P_0 [kN]	50.0	
	Distance from the left end x_0 [m]	2.5	
Load case 2	Concentrated moment M_0 [kN.m]	50.0	
	Distance from the left end x_0 [m]	2.5	

In the present test, parameters β , $\bar{\mu}$ and $\bar{\sigma}$ are respectively set as 0.1, $L/2$ and 0.2. Thus, the element number is the sole parameter controlling the meshing.

Tables 2-3 have recorded the deflections of beam at the mid-span bottom with the refinement of meshing and increase of longitudinal slip stiffness k_p , where the Winkler's spring stiffness k_w is assigned as a constant 3.081 MPa. In the case of thick foundation beam, Table 2 indicates that the mid-span deflection converges so fast to certain stable value that a very decent accuracy can be achieved even when very few of elements are used. Table 2, as a counterpart, deals with the case of slender beam, and it confirms that the solutions of slender foundation beam converge stably with the refinement of meshing, though slower than the case of thick beam. The results of classical beam-foundation system, whose beam is described by TBT or EBT, are also provided in Tables 2-3, aiming to study the relationship between the proposed model and classical ones. It is shown that the results based on EBT underestimate the deflection, while those based on TBT overestimate the deflection, if w_{HBT} is assumed to come closer to the exact solutions.

Slip locking (Dall'Asta and Zona 2004) is a well-known numerical problem, which tends to arise in the partial interaction problem with relative stiff shear interaction, usually in the composite or laminated structures. In fact, the beam-foundation system can also be categorized to composite structure. Thus, the slip locking test has also been carried out in Tables 2-3. From the tables, it is observed that the mid-span deflection of the beam always converges to the case when the second parameter of Pasternak foundation is rigid, which manifests the locking free characteristics of the proposed finite element.

Table 2 Convergence of the proposed higher order foundation beam element, $L = 3H$

k_p/k_w	Mid-span downward deflection [mm]							
	Element number n_e						Analytical solutions	
	1	3	7	15	31	63	TBT	EBT
10^{-5}	5.418	5.427	5.428	5.429	5.429	5.429	5.4304	5.4215
10^2	5.417	5.426	5.427	5.427	5.427	5.427	5.4288	5.4198
10^5	5.413	5.419	5.419	5.419	5.419	5.420	5.4215	5.4126
10^{10}	5.413	5.419	5.419	5.419	5.419	5.419	5.4214	5.4125
no slip	5.413	5.419	5.419	5.419	5.419	5.419	—	—

Table 3 Convergence of the proposed higher order foundation beam element, $L=10H$

k_p/k_w	Mid-span downward deflection [mm]							
	Element number n_e						Analytical solutions	
	1	3	7	15	31	63	TBT	EBT
10^{-5}	1.850	1.952	2.026	2.028	2.029	2.030	2.0316	2.0061
10^2	1.739	1.813	1.849	1.850	1.851	1.852	1.8545	1.8270
10^5	1.690	1.743	1.755	1.755	1.756	1.756	1.7587	1.7303
10^{10}	1.690	1.743	1.755	1.755	1.756	1.756	1.7584	1.7300
no slip	1.690	1.743	1.755	1.755	1.756	1.756	—	—

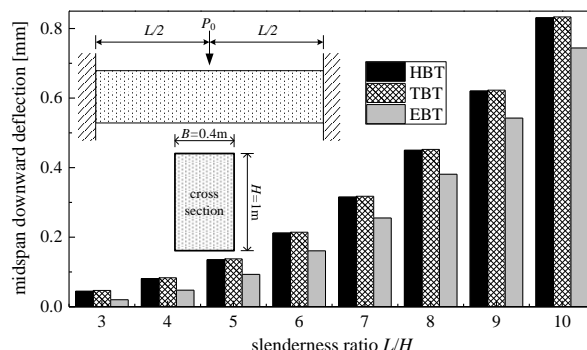


Fig. 5 Prediction of midspan deflection using HBT, TBT and EBT

4.1.2 Shear effects

It is essential to take into account the shear deformation, when predicting the mechanical behaviors of the deep beam structures. As a result, the Timoshenko beam model, as one of the most popular models, was proposed to consider the first order of shear deformation. To have a better understanding of the distribution of shear stress more than the first order, the HBT was proposed. Compared with the Timoshenko model, the Euler-Bernoulli model, however, neglected the shear deformation of the beam.

In this section, the shear effects on the prediction of beam deflection are investigated, using three beam theories: EBT, TBT and HBT. The meshing Eq. (24) are still adopted in this investigation, and the same geometric and physical parameters used in Section 4.1.1 are reused, except for the boundary conditions. Herein, both ends of the beam are clamped and the subgrade reaction is neglected. Fig. 5 presents the mid-span deflections of clamped-clamped beam, with slenderness ratio ranging from 3 to 10. It can be seen that the discrepancies between the results based on HBT and TBT are quite small, while those between results obtained by HBT and EBT are not negligible, due to the shear deformation. The relative errors between the HBT and EBT, however, show to decrease with the increase of the slenderness ratio. Thus, it may be concluded that it should be avoided to use EBT in the analysis of deep beam structures, and the TBT model is good at the deflection prediction.

4.2 Numerical verification and comparison

In order to verify the proposed finite element, several numerical examples are presented, including both linear and nonlinear cases. In the linear examples, two static analyses of beam on Pasternak foundation are performed. One explores the influence of axial deformation on beam's deflection and internal forces, and the other investigates its influence on the stresses. In the nonlinear examples, comparisons with the work of Sapountzakis and Kampitsis (2013) are carried out to demonstrate the reliability of the proposed finite element program.

4.2.1 Linear example 1

In this section, the numerical results of Shirima and Giger (1992) are used as a comparison. The numerical example deals with a Timoshenko beam with free-free boundary conditions (see Table 1) resting on a Pasternak foundation. The load case 2 shown in the table is considered, and the other parameters are also shown in Table 1.

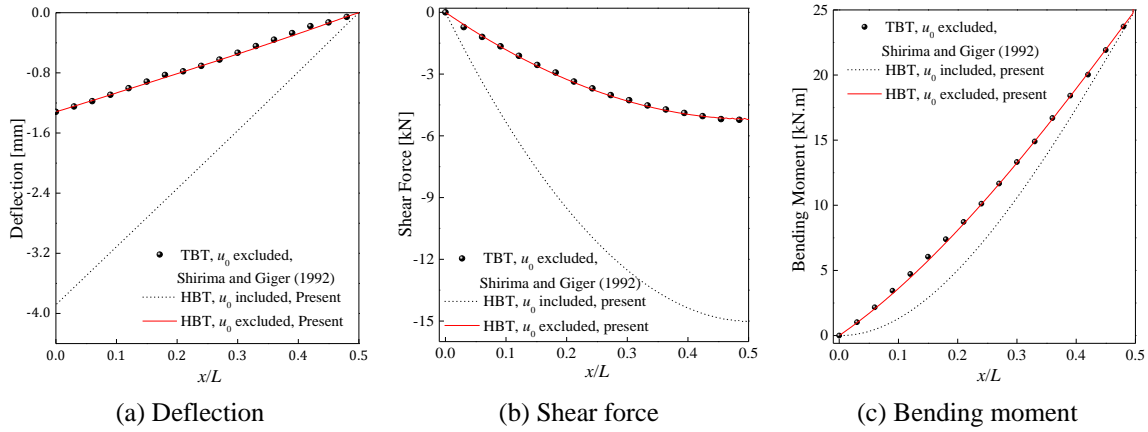


Fig. 6 Influences of the axial deformation

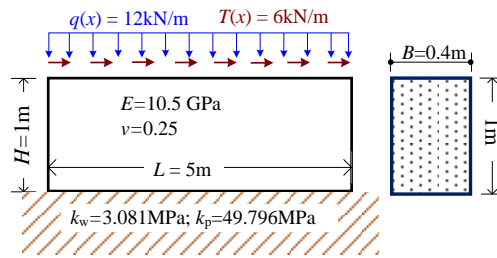


Fig. 7 Structural parameters for numerical example 2

Fig. 6 compares the present results with those of Shirima and Giger (1992), who neglected the longitudinal displacement (denoted as u_0 in the present study) at the centroid axis. It is clearly shown that the results of Shirima and Giger (1992) and the present have a good agreement, if the axial displacement u_0 is also neglected in the proposed HBT model. It is revealed that the Timoshenko's first order shear deformation assumption may achieve a decent fidelity in the analyses of deflection, shear force and bending moment in this case. However, a significant discrepancy between the results arises, if u_0 is considered in the model. Thus, it may be concluded that the centroid's longitudinal deformation influences much on the behavior of the beam on Pasternak foundation, and we guess it may also affect the stress analysis, which, as a result, will be further discussed in Section 4.2.2.

4.2.2 Linear example 2

This example aims to investigate the effects of u_0 on the stress analyses, including axial normal stress, transverse normal stress and shearing stress. As is shown in Fig. 7, the same boundary conditions, geometric and material parameters as Table 1 shows are considered, except for the load case. Herein the top surface of beam is subjected to the uniformly distributed pressure $q(x) = 12$ kN/m and traction $T(x) = 6$ kN/m.

Fig. 8 presents the contours of axial normal stress, where the results based on HBT, TBT and plane stress models are provided in Fig. 8(a). It is observed from the figure that the present HBT model predicts axial normal stress much closer to plane stress model than does the TBT model. Fig.

8(b) in contrast with Fig. 8(a), shows the corresponding results when the centroid's axial displacement is neglected. It can be concluded that the contour discrepancies among different theories demonstrate the significance of u_0 . This might be the reason accounting for the deviation of bending moment caused by the u_0 shown in Fig. 6(c).

Similarly, Figs. 8-9 are devoted to investigating the influences of the centroid's displacement u_0 on the distribution of transverse normal stress and shearing stress. Fig. 9(a) shows a decent convergence of transverse normal stress using plane stress model and the proposed HBT, where the results based on TBT can't be given due to the kinematics itself. The effects of axial deformation are also checked in Fig. 9(b), where the same phenomenon, as expected, is observed that a serious distortion of stress occurs if the u_0 is neglected. Moreover, Fig. 10(a) indicates that the results based on the present HBT and plane stress model almost coincide exactly with each other, whereas the results based on TBT can only capture a uniform distribution of shearing stress due to the first order shear deformation assumption. A further analysis has also been conducted to

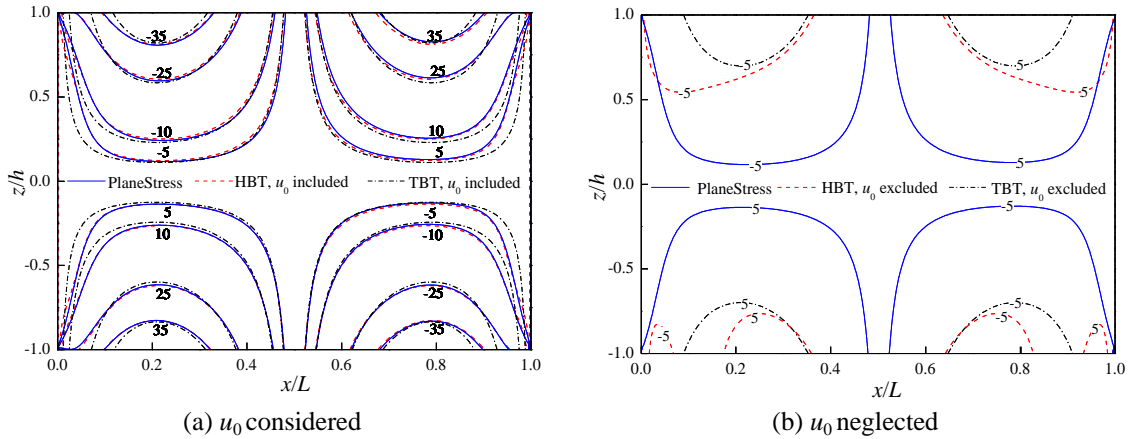


Fig. 8 Contours of axial normal stress in kPa, using the plane stress model, HBT and TBT

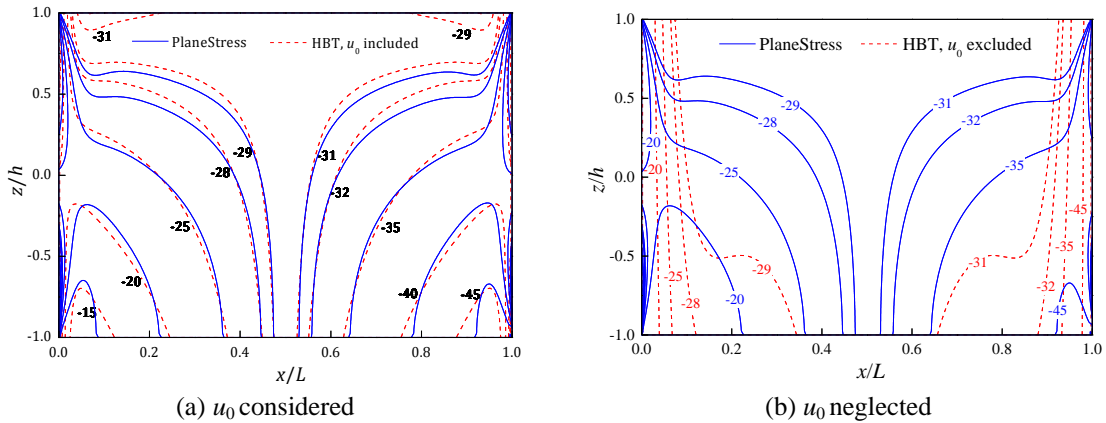


Fig. 9 Contours of transverse normal stress, using the plane stress model and higher order beam model

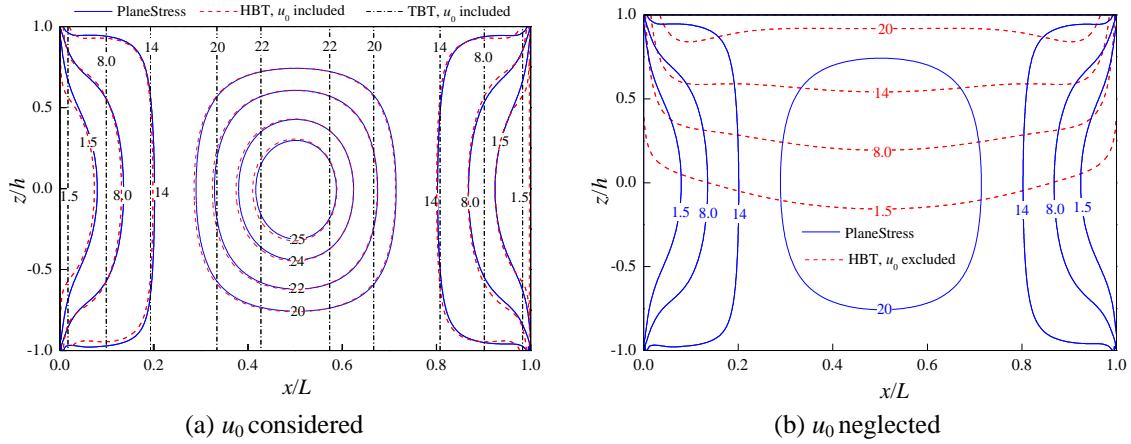


Fig. 10 Contours of shearing stress resulting from plane stress model, HBT and TBT

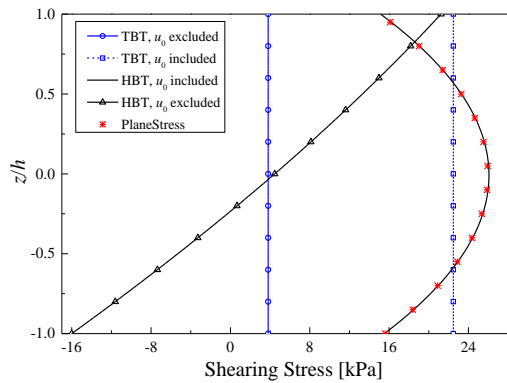


Fig. 11 Shearing stress over the mid-span cross section

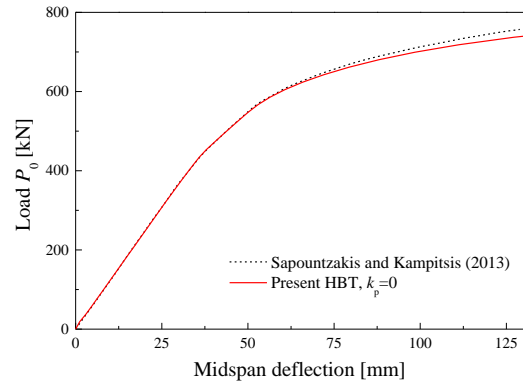


Fig. 12 Load-displacement curve at the mid-point of the beam of nonlinear example 1

examine the distribution of shearing stress over the mid-span cross-section in Fig. 10, where an amazing matching of shearing stress based on the proposed HBT and plane stress model is observed. However, the results neglecting u_0 shown in Fig. 10(b) and 11 manifest an obvious distortion. Thus far, it may be concluded that the centroid's axial displacement should be considered in the stress analysis of beam-foundation system.

4.2.3 Nonlinear example 1

This example, which was previously studied by Sapountzakis and Kampitsis (2013) using the EBT-based boundary element method, is given to verify the reliability of the proposed model and its finite element program on the nonlinear analyses. Herein a simply supported beam of length 7.62 m and square cross-section of side 159.004 mm subjected to a monotonically increasing concentrated vertical load P_0 at its midpoint is studied. The beam is assumed to be elastic-plastic with modulus of elasticity $E = 199.948$ GPa and shear modulus $G = 80$ GPa, yielding stress $\sigma_s = 206.843$ MPa and $\tau_s = 160$ MPa, and a strain hardening slope $E_t = 2.79927$ GPa and $G_t = 1.12$ GPa;

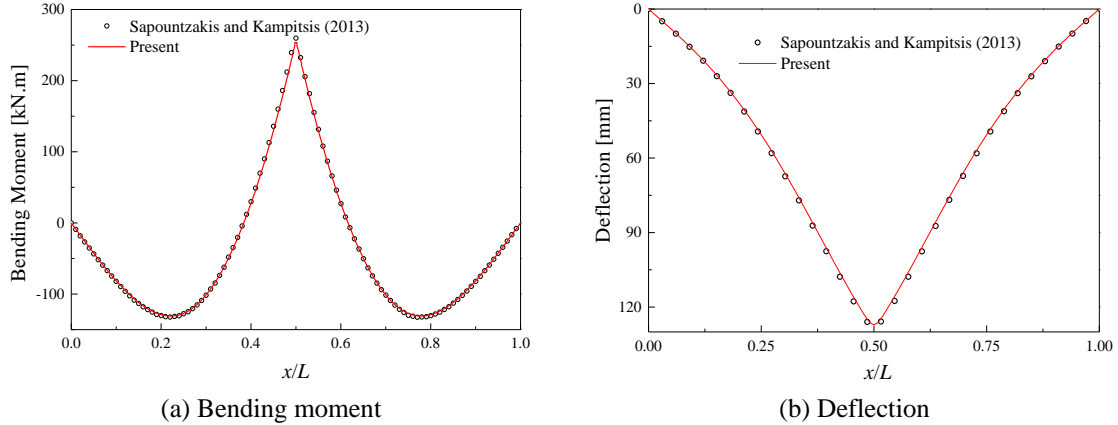


Fig. 13 Numerical results of nonlinear example 1, with mid-span deflection prescribed to be 127 mm

the Winkler foundation p - y curve is also considered to be elastic-plastic with initial stiffness $k_w = 3.44738$ MPa, yielding pressure 175.127 kN/m and a hardening slope $k_{wr} = 34.4738$ kPa. The longitudinal stiffness k_p is neglected in this example. The entire span of the beam is meshed by 101 elements of even length, and five Gauss integration nodes are used for cross-sectional integration; four Gauss integration nodes are used for the longitudinal direction integration.

Fig. 12 presents load-deflection curves of the beam's mid-span obtained by Ref. (Sapountzakis and Kampitsis 2013) and the present model, from which an excellent agreement can be observed when mid-span deflection is less than 50 mm, while the deviation develops with the further increase of deflection. This can be accounted, on the one hand, that the shear effect tends to be negligible for the present very slender beam (whose slenderness ratio is 47.9) in the linear elastic stage, on the other hand, the larger shear deformation results in the decrease of the shear stiffness in the nonlinear stage, which may cause softening of global stiffness shown in Fig. 12. The bending moment and deflection along the beam are presented in Fig. 13, in which the mid-span deflection is prescribed to be 127 mm. The very few of discrepancy shown in the figure again confirms the reliability of the present program.

Table 4 Materials for nonlinear example 2

Materials	Parameters	Perfectly plastic	Strain hardening
Beam	Initial Elastic modulus, E_0 [MPa]	32318.4	32318.4
	Yield strength for normal stress σ_s [MPa]	20.0	20.0
	Harding modulus, E_t [MPa]	0.0	650.0
	Initial shear modulus, G_0 [GPa]		12.80
	Yield strength for shearing stress τ_s [MPa]		25.60
	Harding shear modulus, G_t [MPa]		0.0
Foundation	Initial Stiffness for pressure k_w [MPa]		20.0
	Yield strength for pressure k_{ws} [kN/m]		60.0
	Longitudinal stiffness k_p [MPa]		55.5556

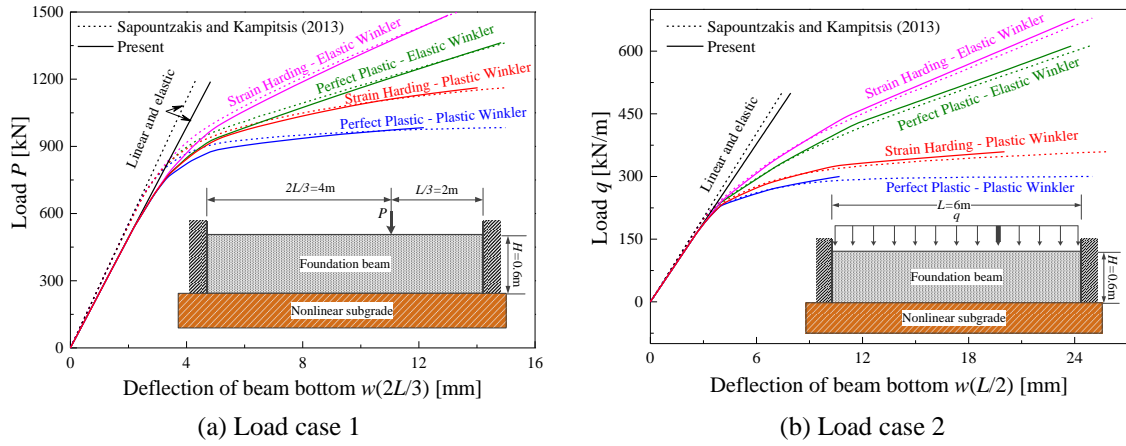


Fig. 14 Load-displacement curve at the mid-point of nonlinear example 2

4.2.4 Nonlinear example 2

In order to carry out a more comprehensive verification of the proposed finite element program, a beam resting on the nonlinear Pasternak foundation is studied. The dimensions of the beam is $H = 0.6$ m, $B = 0.3$ m and $L = 6.0$ m and both of its ends are clamped. There are two types of nonlinear materials shown in Table 4 used for the beam to describe normal strain-stress relationship. One is Perfectly Plastic and the other is Strain Hardening. The behavior of shear deformation is both assumed to follow the perfectly plastic model, which is also shown in Table 4. Furthermore, two types of foundation are used in the example: one is elastic Pasternak with the initial stiffness parameters shown in Table 4 throughout the entire working stage, and the other is Perfectly Plastic with yield strength 60 kN/m.

Sapoutzakis and Kampitsis (2013) had also studied this example using the boundary element method, where the EBT was used in their model. There are two load cases analyzed in the example, which are shown in Figs. 14(a) and (b), respectively, and the same scheme of element integration

Table 5 Geometric and materials parameters for Section 4.3

		Materials	Parameters	Value
	Beam		Initial Elastic modulus, E_0 [GPa]	200
			Yield strength for normal stress σ_s [MPa]	207
			Harding modulus, E_t [GPa]	2.8
			Initial shear modulus, G_0 [GPa]	80
			Yield strength for shearing stress τ_s [MPa]	160
			Harding shear modulus, G_t [MPa]	1.12
Foundation			Initial Stiffness for pressure k_w [MPa]	8.0
			Yield strength for pressure k_{ws} [kN/m]	200
			Initial longitudinal stiffness k_p [MPa]	50
			Coefficient of sliding friction	0.85 or 0.3

and meshing are used as those used in Section 4.2.3. The force incremental technique is applied to this example and the results are shown in Fig. 14, from which it can be observed that the global stiffness in the linear stage decreases, due to the refinement of beam kinematics, whichever combination of materials the soil-foundation system adopts. Thus, the finite element program implemented, to some extent, is verified by the good consistence of overall load-displacement curves generated by HBT and EBT.

4.3 Effects of friction and tensionless characteristics

In this section, the effects of interfacial interaction between the beam and foundation as well as the tensionless (Sapountzakis and Kampitsis 2013) feature of the foundation are studied through two numerical examples. Herein a foundation beam with dimensions $B = 0.3$ m, $H = 1$ m and $L = 20$ m (see Table 5) is resting on the nonlinear foundation, and is subjected to point loads at the midpoint of beam. The beam and foundation are assumed to be strain hardening and perfectly plastic, respectively, whose detailed parameters are listed in Table 5. Based on these parameters, extensive quasi-static analyses are carried out in the following sub-sections.

4.3.1 Effects of friction

The vertical ultimate bearing capacity at the midpoint of beam P_u is obtained from the load-displacement curve shown in Fig. 15, assuming $T_0 = 0$, $M_0 = 0$ and the coefficient of sliding friction $\mu = 0.85$. From the figure, a P_u of quantity 4000 kN is determined. Subsequently, the pressure reactions of the foundation under three load levels $P_0 = 0.2P_u$, $P_0 = 0.5P_u$ and $P_0 = 0.8P_u$ are respectively captured and shown in Fig. 16. It can be approximately judged from Fig. 15 that the structure's mechanical behavior is linear in the load levels $P_0 = 0.2P_u$ and $P_0 = 0.5P_u$, whereas it manifests obvious nonlinearity when $P_0 = 0.8P_u$. Accordingly, the reaction responding to $P_0 = 0.2P_u$ and $P_0 = 0.5P_u$ (see Fig. 16), is of proportion very close to 2:5. And the reaction responding to level $P_0 = 0.8P_u$ turns out to be definitely unproportional to the results resulting from the previous two load levels.

The influence of interfacial friction on the longitudinal bearing capacity is illustrated in Fig. 17, where the previously used three load levels are considered. Herein the u_0 of the mid-span cross-section is chosen as the controlling DOF in the displacement incremental technique and the

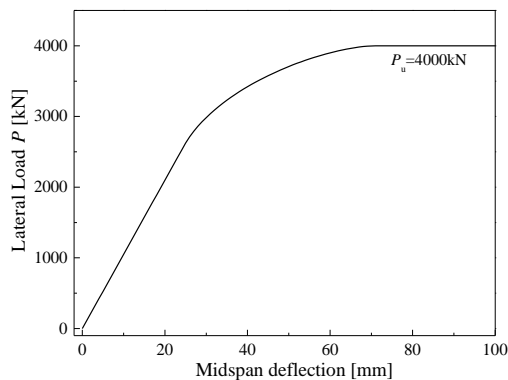


Fig. 15 Load-displacement curve at the midpoint with $T_0 = 0$ and $\mu = 0.85$

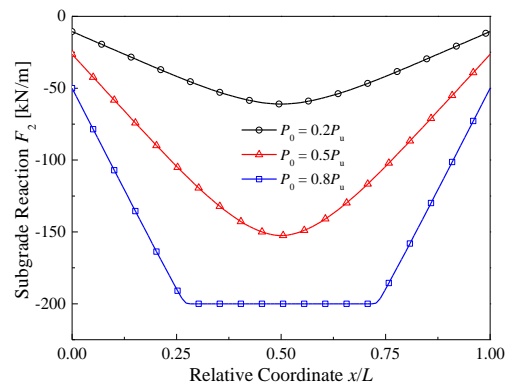


Fig. 16 Distribution of foundation pressure with $T_0 = 0$ and $\mu = 0.85$

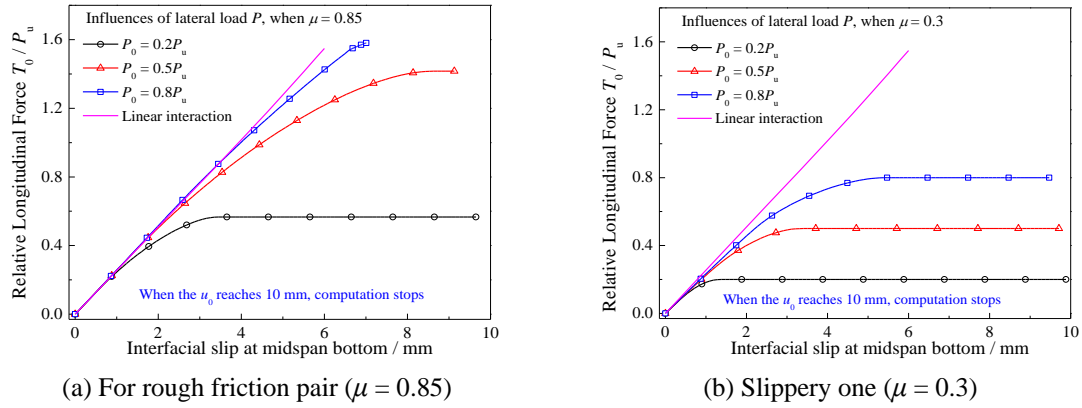


Fig. 17 Longitudinal force T_0 vs. interfacial slip at mid-span bottom, with different coefficients of sliding friction and pressure levels P_0

program runs until u_0 reaches 10 mm. It can be clearly seen that the longitudinal bearing capacity increases significantly with the increase of vertical load P_0 , which can be accounted that the increase of interfacial pressure, as is shown in Fig. 16, improves the sliding strength of the friction pair. The comparison of Figs. 17(a) and (b) carries on confirming that the ultimate longitudinal bearing force can be elevated by roughening the surfaces of the friction pair. The results based on elastic longitudinal interfacial interaction are also presented in the figure, from which it can be concluded that a serious overestimation of longitudinal bearing force may arise in the case when the vertical load is small or the friction interface is not very rough.

4.3.2 Effects of tensionless characteristics

This example is presented to demonstrate the significance of the tensionless characteristics in the analyses and design. Herein it is assumed that $P_0 = 800$ kN, $T_0 = 0$ and $\mu = 0.85$. From Fig. 18, it can be seen that the ultimate bearing capacity of external moment M_0 would be magnified from $M_{u1} = 6399.42$ kN·m to $M_{u2} = 19194.02$ kN·m, that is almost an overestimation of 200%, if the foundation is capable of resisting tension and the function $F_2(w)$ is symmetric with respect to the

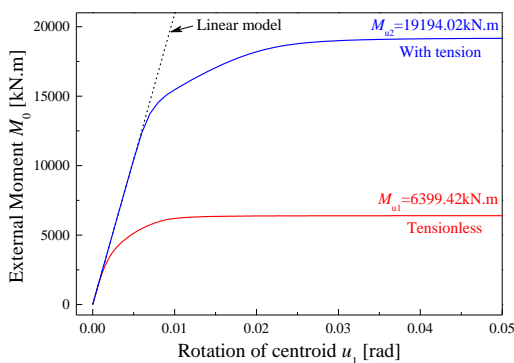


Fig. 18 Influence of the interfacial tension on the load-displacement curve

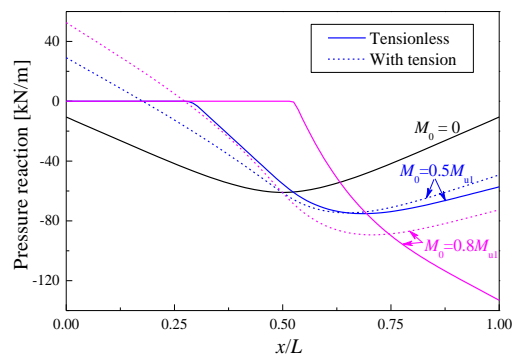


Fig. 19 Effects of tensionless characteristics of foundation on the foundation pressure along the beam

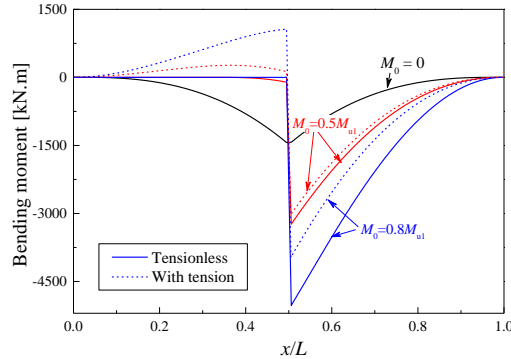


Fig. 20 Effects of tensionless characteristics on the distribution of bending moment along the beam length

origin of the p - y curve. Furthermore, it is illustrated that the linear range of load-displacement curve may be conspicuously extended by the extra tension, judging from the curve of linear Pasternak model.

Figs. 19 and 20 are presented to illustrate the significance of the tensionless characteristics of the foundation, where $P_0 = 800$ kN, $T_0 = 0$ and three load levels of $M_0 = 0$, $M_0 = 0.5M_{u1}$ and $M_0 = 0.8M_{u1}$ are considered. It can be observed from Fig. 19 that the pressure reaction of the foundation along the left half span decreases with the increase of concentrated external moment M_0 , if the tensionless property of foundation is considered. There, however, arises interface in tension in the vicinity of the left end of the beam, and the region is to extend with the increase of external moment. Moreover, an increasing underestimation of foundation pressure, due to the extra tension, can also be observed. Fig. 20 examines the bending moment of the beam responding to the external moment, and it can be seen that bending moment decreases with the increase of external moment, if the tensionless characteristics of the soil is considered. Whereas, a hogging region arises in the left half span of the beam, when $M_0 = 0.5M_{u1}$ or $M_0 = 0.8M_{u1}$, if the foundation can resist tension. Thus far, it has been illustrated that the tensionless property of the beam-foundation interface is a factor of crucial importance in the analysis and design.

4.4 CPU time and memory issues

CPU time cost is an essential factor in the analysis of the foundation beam. As far as the computation examples above performed, the total degrees of freedom is really small compared with the 2D elements like the quadrilateral plane stress elements or 3D hexahedral solid elements. Moreover, the beam on foundation can usually be discreted with not much of elements (63 for instance in Section 4.1.1). Therefore, the CPU time and memory requirement could not be the factor hinders the present finite element analysis.

5. Conclusions

In this paper, a new type of higher order beam model, which provides both longitudinal and transversal displacements and stresses, is proposed. And the model is applied to the nonlinear beam-foundation system problem, where the beam-foundation interaction is described by Masing's

friction law and Pasternak's foundation model on the one hand and the nonlinear material of beam are also considered on the other. Then, the corresponding finite element for the proposed model is formulated and verified by the comparison with the existed results of Refs. (Shirima and Giger 1992, Sapountzakis and Kampitsis 2013) and those based on classical Pasternak beam-foundation system. The convergence performance of the proposed element is conducted, showing that the present element is locking free. Finally, extensive quasi-static analyses are performed to study the influences of tensionless property and friction on the mechanical behavior. Through this study, the following main conclusions can be drawn:

- (1) The proposed higher order beam model can be a good candidate for detailed analysis of beam structures.
- (2) The DOF of u_0 , on the one hand, influences much on the mechanical behavior of the beams, including displacement and internal-force results, on the other hand, a serious distortion of stress resultants may arise without this DOF.
- (3) The tensionless and friction characteristics of the beam-foundation interface shall be considered, or an underestimation of foundation pressure reaction and bending moment may arise.

References

- Al-Bender, F., Lampaert, V. and Swevers, J. (2005), "The generalized Maxwell-slip model: a novel model for friction simulation and compensation", *IEEE T. Automat. Control*, **50**(11), 1883-1887.
- Ayoub, A. (2003), "Mixed formulation of nonlinear beam on foundation elements", *Comput. Struct.*, **81**(7), 411-421.
- Batoz, J.L. and Dhatt, G. (1979), "Incremental displacement algorithms for nonlinear problems", *Int. J. Numer. Meth. Eng.*, **14**(8), 1262-1267.
- Berger, E.J. (2002), "Friction modeling for dynamic system simulation", *App. Mech. Rev.*, **55**(6), 535-577.
- Chen, W.Q., Lv, C.F. and Bian, Z.G. (2004), "A mixed method for bending and free vibration of beams resting on a Pasternak elastic foundation", *Appl. Math. Model.*, **28**(10), 877-890.
- Comodromos, E.M. and Bareka, S.V. (2005), "Evaluation of negative skin friction effects in pile foundations using 3D nonlinear analysis", *Comput. Geotech.*, **32**(3), 210-221.
- Comodromos, E. M. and Papadopoulou, M.C. (2013), "Explicit extension of the p-y method to pile groups in cohesive soils", *Comput. Geotech.*, **47**(1), 28-41.
- Dall'Asta, A. and Zona, A. (2004), "Slip locking in finite elements for composite beams with deformable shear connection", *Finite Elem. Anal. Des.*, **40**(13-14), 1907-1930.
- Dash, S.R., Govindaraju, L. and Bhattacharya, S. (2009), "A case study of damages of the Kandla Port and Customs Office tower supported on a mat-pile foundation in liquefied soils under the 2001 Bhuj earthquake", *Soil Dyn. Earthq. Eng.*, **29**(2), 333-346.
- Dutta, S.C. and Roy, R. (2002), "A critical review on idealization and modeling for interaction among soil-foundation-structure system", *Comput. Struct.*, **80**(20), 1579-1594.
- Feng, Z. and Cook, R.D. (1983), "Beam elements on two-parameter elastic foundation", *J. Eng. Mech., ASCE*, **109**(6), 1390-1402.
- Georgiadis, K. and Georgiadis, M. (2012), "Development of p-y curves for undrained response of piles near slopes", *Comput. Geotech.*, **40**(3), 53-61.
- Han, S.M., Benaroya, H. and Wei, T. (1999), "Dynamics of transversely vibrating beams using four engineering theories", *J. Sound Vib.*, **225**(5), 935-988.
- Jones, R. and Xenophontos, J. (1977), "The vlasov foundation model", *Int. J. Mech. Sci.*, **19**(6), 317-323.
- Masing, G. (1923), *Zur Heyn'schen Theorie der Verfestigung der Metalle durch verborgen elastische*

- Spannungen*, Springer.
- Mullapudi, R. and Ayoub, A. (2010), "Nonlinear finite element modeling of beams on two-parameter foundations", *Comput. Geotech.*, **37**(3), 334-342.
- Nobili, A. (2013), "Superposition principle for the tensionless contact of a beam resting on a Winkler or a Pasternak foundation", *J. Eng. Mech., ASCE*, **139**(10), 1470-1478.
- Nogami, T. and O'Neill, M.W. (1985), "Beam on generalized two-parameter foundation", *J. Eng. Mech., ASCE*, **111**(5), 664-679.
- Popp, K., Panning, L. and Sextro, W. (2003), "Vibration damping by friction forces: Theory and applications", *J. Vib. Control*, **9**(3-4), 419-448.
- Sapountzakis, E.J. and Kampitsis, A.E. (2011a), "Nonlinear analysis of shear deformable beam-columns partially supported on tensionless three-parameter foundation", *Arch. Appl. Mech.*, **81**(12), 1833-1851.
- Sapountzakis, E.J. and Kampitsis, A.E. (2011b), "Nonlinear response of shear deformable beams on tensionless nonlinear viscoelastic foundation under moving loads", *J. Sound Vib.*, **330**(22), 5410-5426.
- Sapountzakis, E.J. and Kampitsis, A.E. (2013), "Inelastic analysis of beams on two-parameter tensionless elastoplastic foundation", *Eng. Struct.*, **48**, 389-401.
- Shirima, L.M. and Giger, M.W. (1992), "Timoshenko beam element resting on two-parameter elastic foundation", *J. Eng. Mech., ASCE*, **118**(2), 280-295.
- Winkler, E. (1867), *Theory of Elasticity and Strength*, Dominicus Prague.
- Zhang, Y. and Murphy, K.D. (2013), "Tensionless contact of a finite beam: Concentrated load inside and outside the contact zone", *Acta Mech. Sinica*, **29**(6), 836-839.
- Zhou, H., Luo, S. and Sun, D. (2011), "The bending analysis of a beam on elastic foundation with large deflection including the effects of horizontal friction", *Eng. Mech.*, **28**(1), 43-54.
- Zienkiewicz, O.C. and Taylor, R.L. (2000), *The Finite Element Method*, (Fifth Edition), Volume 2: Solid Mechanics, Butterworth-Heinemann.

Appendix A

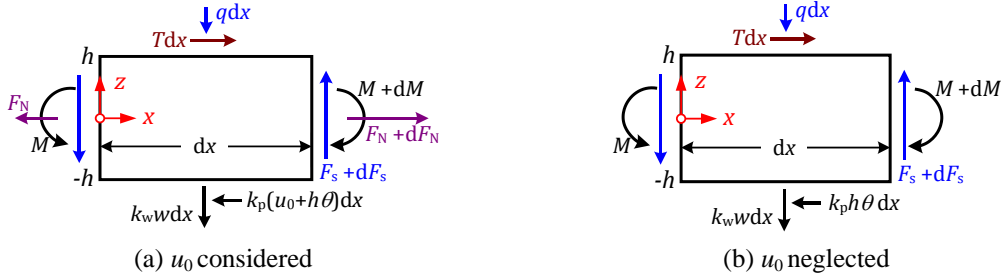


Fig. 21 Infinitesimal element for the Timoshenko beam on Pasternak foundation

A.1 Timoshenko beam on Pasternak foundation

For Timoshenko beam on Pasternak foundation, where the centroid's axial displacement u_0 is considered (see Fig. 21(a)), the displacement based governing differential equations can be formulated as

$$\begin{cases} kGA(w'' - \theta') - q - k_w w = 0 \\ -EI\theta'' + Th + k_p h(u_0 + \theta h) - kGA(w' - \theta) = 0 \\ EAu_0'' + T - k_p(u_0 + \theta h) = 0 \end{cases} \quad (\text{A.1})$$

and force boundary conditions

$$\begin{cases} \bar{M} = -EI\theta' \\ \bar{F}_s = kGA(w' - \theta), \quad x = 0 \text{ or } L \\ \bar{F}_N = EAu_0' \end{cases} \quad (\text{A.2})$$

hereafter, symbols \bar{M} , \bar{F}_s and \bar{F}_N denote the external force acting on the boundary $x=0$ or L .

For the free-free boundary conditions, $\bar{M} = 0$, $\bar{F}_s = 0$ and $\bar{F}_N = 0$, at both $x = 0$ and L ; k , G , A and I are Timoshenko shearing stress correction factor (herein $k = 5/6$), shear modulus, area of the cross-section and moment of inertia, respectively.

In the case when u_0 is neglected (see Fig. 21(b)), the governing differential equations can be expressed as

$$\begin{cases} kGA(w'' - \theta') - q - k_w w = 0 \\ -EI\theta'' + Th + k_p h^2 \theta - kGA(w' - \theta) = 0 \end{cases} \quad (\text{A.3})$$

and force boundary conditions

$$\begin{cases} \bar{M} = -EI\theta' \\ \bar{F}_s = kGA(w' - \theta) \end{cases}, \quad x = 0 \text{ or } L \quad (\text{A.4})$$

A.2 Euler-Bernoulli beam on Pasternak foundation

For Euler-Bernoulli beam on Pasternak foundation, an additional kinematic constraint shall be introduced as $\theta = w'$. Subsequently, the displacement based governing differential equations considering u_0 can be reduced to

$$\begin{cases} EIw^{(4)} - k_p hu'_0 + k_w w + q - k_p h^2 w'' = 0 \\ EAu''_0 - k_p (u_0 + hw') + T = 0 \end{cases} \quad (\text{A.5})$$

and force boundary conditions

$$\begin{cases} \bar{M} = -EIw'' \\ \bar{F}_s = -EIw''' + Th + k_p h^2 w' + k_p hu_0 \end{cases}, \quad x = 0 \text{ or } L \quad (\text{A.6})$$

If u_0 is neglected, Eqs. (A.5)-(A.6) will be reduced to the follows

$$EIw^{(4)} + k_w w + q - k_p h^2 w'' = 0 \quad (\text{A.7})$$

and force boundary conditions

$$\begin{cases} \bar{M} = -EIw'' \\ \bar{F}_s = -EIw''' + Th + k_p h^2 w' \end{cases}, \quad x = 0 \text{ or } L \quad (\text{A.8})$$

All the above differential equations are linear boundary value problems, and they can be directly solved by computer algebra system. Herein, these equations are analytically solved by *Mathematica*.